Biochemical and Biophysical Research Communications 430 (2013) 1301–1305

Contents lists available at SciVerse ScienceDirect

Biochemical and Biophysical Research Communications

journal homepage: www.elsevier.com/locate/ybbrc

Reductive nitrosylation of *Methanosarcina acetivorans* protoglobin: A comparative study

Paolo Ascenzi [a,b,*], Alessandra Pesce [c], Marco Nardini [d], Martino Bolognesi [d], Chiara Ciaccio [e,f], Massimo Coletta [e,f], Sylvia Dewilde [g]

[a] *Laboratorio Interdipartimentale di Microscopia Elettronica, Università Roma Tre, Via della Vasca Navale 79, I-00146 Roma, Italy*
[b] *Istituto di Biochimica delle Proteine, CNR, Via Pietro Castellino 111, I-80131 Napoli, Italy*
[c] *Dipartimento di Fisica, Università di Genova, I-16146 Genova, Italy*
[d] *Dipartimento di Bioscienze, Università di Milano, Via Celoria 26, I-20133 Milano, Italy*
[e] *Dipartimento di Scienze Cliniche e Medicina Traslazionale, Università di Roma Tor Vergata, Via Montpellier 1, I-00133 Roma, Italy*
[f] *Consorzio Interuniversitario di Ricerca in Chimica dei Metalli nei Sistemi Biologici, Piazza Umberto I 1, I-70121 Bari, Italy*
[g] *Department of Biomedical Sciences, University of Antwerp, Universiteitsplein 1, B-2610 Antwerp, Belgium*

ARTICLE INFO

Article history:
Received 9 November 2012
Available online 19 December 2012

Keywords:
Methanosarcina acetivorans protoglobin
Reductive nitrosylation of ferric *Methanosarcina acetivorans* protoglobin
Nitrosylation of ferrous *Methanosarcina acetivorans* protoglobin
Kinetics
Thermodynamics

ABSTRACT

Methanosarcina acetivorans is a strictly anaerobic non-motile methane-producing Archaea expressing protoglobin (Pgb) which might either facilitate O_2 detoxification or act as a CO sensor/supplier in methanogenesis. Unusually, *M. acetivorans* Pgb (*Ma*Pgb) binds preferentially O_2 rather than CO and displays anticooperativity in ligand binding. Here, kinetics and/or thermodynamics of ferric and ferrous *Ma*Pgb (*Ma*Pgb(III) and *Ma*Pgb(II), respectively) nitrosylation are reported. Data were obtained between pH 7.2 and 9.5, at 22.0 °C. Addition of NO to *Ma*Pgb(III) leads to the transient formation of *Ma*Pgb(III)–NO in equilibrium with *Ma*Pgb(II)–NO^+. In turn, *Ma*Pgb(II)–NO^+ is converted to *Ma*Pgb(II) by OH^--based catalysis. Then, *Ma*Pgb(II) binds NO very rapidly leading to *Ma*Pgb(II)–NO. The rate-limiting step for reductive nitrosylation of *Ma*Pgb(III) is represented by the OH^--mediated reduction of *Ma*Pgb(II)–NO^+ to *Ma*Pgb(II). Present results highlight the potential role of *Ma*Pgb in scavenging of reactive nitrogen and oxygen species.

1. Introduction

Phylogenetic analysis revealed that three globin lineages probably evolved from an ancestral flavo-hemoglobin-like single-domain protein. The first lineage includes flavo-hemoglobins and related single domain globins (e.g., myoglobin; Mb). The second lineage comprises truncated hemoglobins showing the 2-on-2 α-helical fold. The third lineage encompasses two-domain globin-coupled sensors, single-domain sensor globins, and related single-domain protoglobins (Pgb) [1–6].

Pgbs are homodimers, each subunit being composed by approximately 195 amino acids, which are related to the N-terminal domain of archaeal and bacterial globin-coupled sensor proteins [1–6]. The elucidation of the three-dimensional structure of *Methanosarcina acetivorans* protoglobin (*Ma*Pgb) revealed that the subunits of Pgbs are structurally related to single-chain globins (e.g., Mb) and to the heme-based aerotaxis transducer sensor domain of *Bacillus subtilis* globin-coupled sensor, being folded into the classical 3-on-3 α-helical sandwich, which is however somewhat extended in its N- and C-terminal regions [7,8]. Since Pgb-specific loops and the N-terminal extension completely bury the heme within the protein matrix, the ligand access to the heme distal pocket is permitted by the Pgb-specific apolar tunnels located at the B/G and B/E α-helix interfaces [7–9].

Up to now, Pgbs have been identified in both Archaea and Bacteria [1–6,10]. Although their function(s) is openly debated, Pgbs might either facilitate O_2 detoxification or act as CO sensor/supplier in methanogenesis [1–6,10]. Unusually, *Ma*Pgb shows a selectivity ratio for O_2/CO binding that favors O_2 ligation and anticooperativity in ligand binding [7,11]. This feature could be related to the fact that *M. acetivorans* takes advantage of acetate,

Abbreviations: Hb, hemoglobin; HPX–heme–Fe, hemopexin–heme–Fe; HSA–heme–Fe, human serum heme–albumin; Lb, leghemoglobin; *Ma*Pgb, *Methanosarcina acetivorans* protoglobin; *Ma*Pgb(III), ferric *Ma*Pgb; *Ma*Pgb(III)–NO, nitrosylated *Ma*Pgb(III); *Ma*Pgb(II), ferrous *Ma*Pgb; *Ma*Pgb(II)-NO, nitrosylated *Ma*Pgb(II); Mb, myoglobin; Ngb, neuroglobin; bis–tris propane, 1,3-bis(tris(hydroxymethyl)-methylamino)propane.

* Corresponding author at: Laboratorio Interdipartimentale di Microscopia Elettronica, Università Roma Tre, Via della Vasca Navale 79, I-00146 Roma, Italy. Fax: +39 06 57336321.
E-mail address: ascenzi@uniroma3.it (P. Ascenzi).

0006-291X/$ - see front matter © 2012 Elsevier Inc. All rights reserved.
http://dx.doi.org/10.1016/j.bbrc.2012.11.122

methanol, CO_2, and CO as carbon sources for methanogenesis; methane production occurs simultaneously with the formation of a proton gradient that is essential for energy harvesting [10,12,13]. Therefore, the ability to convert CO to methane might indicate that CO is the actual ligand of *Ma*Pgb "*in vivo*", supporting the hypothesis of a very ancient origin for such metabolic pathway(s) [10,14].

Here, kinetics and thermodynamics of ferric and ferrous *Ma*Pgb (*Ma*Pgb(III) and *Ma*Pgb(II), respectively) nitrosylation are reported. Reductive nitrosylation of *Ma*Pgb(III) highlights the potential role of Pgbs in scavenging of reactive nitrogen and oxygen species.

2. Materials

*Ma*Pgb was expressed in *Escherichia coli* cells Bl21(DE3)pLysS and collected as described previously [7,15]. *Ma*Pgb(III) was prepared by adding very few grains of ferrycyanide to the *Ma*Pgb solution (1.3×10^{-6} and 2.4×10^{-6} M). *Ma*Pgb(II) was prepared by adding very few grains of sodium dithionite to the *Ma*Pgb(III) solution, under anaerobic conditions. *Ma*Pgb(II)–NO was prepared by adding NO (5.0×10^{-6} M $\leqslant$ [NO] $\leqslant$ 1.0×10^{-3} M) solution to either *Ma*Pgb(III) or *Ma*Pgb(II) solution, and by keeping in a closed vessel either *Ma*Pgb(III) or *Ma*Pgb(II) solution under purified NO, at 760.0 mmHg. The *Ma*Pgb concentration was determined spectrophotometrically using the extinction coefficient of the *Ma*Pgb(II) derivative (*i.e.*, $\varepsilon = 1.25 \times 10^5$ M^{-1} cm^{-1} at 432 nm) [11].

1,3-Bis(tris(hydroxymethyl)methylamino)propane (bis–tris propane) was obtained from Sigma–Aldrich (St. Louis, MO, USA). Gaseous NO was purchased from Aldrich Chemical Co. (Milwaukee, WI, USA) and purified by flowing through a NaOH column in order to remove acidic nitrogen oxides. The NO stock solution was prepared anaerobically by keeping in a closed vessel distilled water under purified NO, at 760.0 mmHg and 20.0 °C. The solubility of NO in the water is 2.05×10^{-3} M, at 760.0 mmHg and 20.0 °C [16]. The NO stock solution was diluted with degassed 1.0×10^{-1} M bis–tris propane buffer (pH 7.2–9.5) to reach the desired concentration (5.0×10^{-6} M $\leqslant$ [NO] $\leqslant$ 1.0×10^{-3} M).

3. Methods

Kinetics and thermodynamics of *Ma*Pgb(III) and *Ma*Pgb(II) nitrosylation between pH 7.2 and 9.5 were fitted to the minimum reaction mechanism represented by Scheme 1 [17–22].

Values of the pseudo-first-order rate constants k^{obs} and h^{obs} (see reactions *a* and *c* in Scheme 1, respectively), and of the dissociation equilibrium constant K ($= k_{off}/k_{on}$; see reaction *a* in Scheme 1) for *Ma*Pgb(III) reductive nitrosylation were obtained by mixing the *Ma*Pgb(III) solution (final concentration and 2.4×10^{-6} M) with the NO solution (final concentration, 2.5×10^{-5} to 1.0×10^{-3} M) under anaerobic conditions. No gaseous phase was present.

$$Ma\text{Pgb(III)} + \text{NO} \underset{k_{off}}{\overset{k_{on}}{\leftrightarrow}} Ma\text{Pgb(III)-NO} \qquad (a)$$

$$Ma\text{Pgb(III)-NO} \overset{fast}{\longleftrightarrow} Ma\text{Pgb(II)-NO}^{+} \qquad (b)$$

$$Ma\text{Pgb(II)-NO}^{+} + \text{OH}^{-} \xrightarrow{h_{OH^-}} Ma\text{Pgb(II)} + \text{HNO}_2 \qquad (c)$$

$$Ma\text{Pgb(II)} + \text{NO} \underset{l_{off}}{\overset{l_{on}}{\leftrightarrow}} Ma\text{Pgb(II)-NO} \qquad (d)$$

Scheme 1. *Ma*Pgb nitrosylation mechanism.

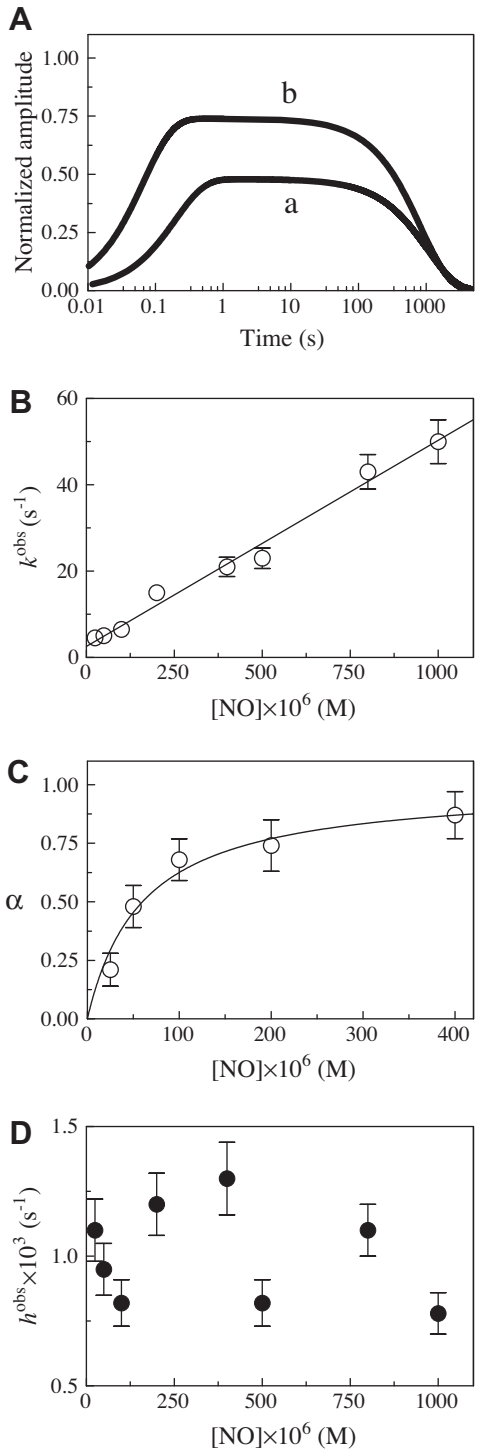

Fig. 1. *Ma*Pgb(III) reductive nitrosylation, at pH 7.2 and 22.0 °C. (A) Normalized averaged time courses of *Ma*Pgb(III) reductive nitrosylation. The NO concentration was 5.0×10^{-5} M (trace a) and 2.0×10^{-4} M (trace b). The time course analysis according to Eqs. (1)–(3) allowed the determination of the following values of parameters α, k^{obs}, and h^{obs}: trace a – $\alpha = 0.48$, $k^{obs} = 5.1$ s^{-1}, and $h^{obs} = 9.5 \times 10^{-4}$ s^{-1}; and trace b – $\alpha = 0.74$, $k^{obs} = 15.0$ s^{-1}, and $h^{obs} = 1.2 \times 10^{-3}$ s^{-1}. (B) Dependence of k^{obs} on [NO] for *Ma*Pgb(III) reductive nitrosylation. The continuous line was generated from Eq. (4) with $k_{on} = (4.8 \pm 0.5) \times 10^4$ M^{-1} s^{-1} and $k_{off} = (2.6 \pm 0.3)$ s^{-1}. (C) Dependence of α on [NO] for *Ma*Pgb(III) reductive nitrosylation. The continuous line was generated from Eq. (5) with $K = (6.0 \pm 0.7) \times 10^{-5}$ M. (D) Dependence of h^{obs} on [NO] for *Ma*Pgb(III) reductive nitrosylation. The average h^{obs} value is 1.0×10^{-3} s^{-1}. The *Ma*Pgb(III) concentration was 2.4×10^{-6} M. Where not shown, standard deviation is smaller than the symbol. For details, see text.

Table 1
Values of kinetic and thermodynamic parameters for nitrosylation of ferric and ferrous *Ma*Pgb, at 22.0 °C.

pH	k_{on} (M^{-1} s^{-1})	k_{off} (s^{-1})	K (M)	k_{off}/k_{on} (M)	h^{obs} (s^{-1})	l_{on} ($M^{-1}s^{-1}$)
7.2	4.8×10^4	2.6	6.1×10^{-5}	5.4×10^{-5}	1.0×10^{-3}	2.7×10^7
7.8	2.6×10^4	8.9×10^{-1}	3.2×10^{-5}	3.4×10^{-5}	2.4×10^{-3}	n.d.
8.5	3.1×10^4	9.1×10^{-1}	4.1×10^{-5}	2.9×10^{-5}	8.5×10^{-3}	2.1×10^7
9.2	4.2×10^4	1.6	2.8×10^{-5}	3.8×10^{-5}	4.7×10^{-2}	n.d.
9.5	3.7×10^4	1.7	4.6×10^{-5}	4.6×10^{-5}	9.0×10^{-2}	3.6×10^7

*Ma*Pgb(III) reductive nitrosylation was monitored between 370 and 450 nm.

Values of the pseudo-first-order rate constants k^{obs} and h^{obs} were obtained according to Eqs. (1)–(3) [17–23]:

$$[\text{MaPgb(III)}]_t = [\text{MaPgb(III)}]_i \times e^{-\text{kobs}\times t} \quad (1)$$

$$[\text{MaPgb(III)} - \text{NO}]_t = [\text{MaPgb(III)}]_i \times (k^{obs} \times ((e^{-\text{kobs}\times t}/(h^{obs} - k^{obs})) + (e^{-\text{hobs}\times t}/(k^{obs} - h^{obs})))) \quad (2)$$

$$[\text{MaPgb(II)} - \text{NO}]_t = [\text{MaPgb(III)}]_i - [\text{MaPgb(III)}]_t + [\text{MaPgb(III)} - \text{NO}]_t \quad (3)$$

Values of k_{on} and k_{off} (reaction *a* in Scheme 1) were determined from the dependence of k^{obs} on [NO], according to Eq. (4) [17–22]:

$$k^{obs} = k_{on} \times [\text{NO}] + k_{off} \quad (4)$$

Values of K (= k_{off}/k_{on}; reaction *a* in Scheme 1) were determined from the dependence of α (i.e., the molar fraction of ligand-bound protein) on [NO], according to Eq. (5) [17–22]:

$$\alpha = [\text{NO}]/(\text{K} + [\text{NO}]) \quad (5)$$

The value of the second-order rate constant h_{OH^-} (see reaction *c* in Scheme 1) for OH^--catalyzed conversion of *Ma*Pgb(II)-NO^+ to *Ma*Pgb(II) was determined from the dependence of h^{obs} on [OH^-] according to Eq. (6) [17–22]:

$$h^{obs} = h_{OH^-} \times [OH^-] + h_{H_2O} \quad (6)$$

where h_{H_2O} is the first-order rate constant for H_2O-catalyzed conversion of *Ma*Pgb(II)–NO^+ to *Ma*Pgb(II).

*Ma*Pgb(III) reductive nitrosylation was also obtained anaerobically by keeping the *Ma*Pgb(III) solution under purified gaseous NO (760 mmHg), at pH 7.2 and 9.2 (1.0×10^{-1} M bis–tris propane buffer) and 22.0 °C [17–22].

Values of the second-order rate constant l_{on} (see reaction *d* in Scheme 1) for *Ma*Pgb(II) nitrosylation were determined from the dependence of l^{obs} on [NO], according to Eq. (7) [16]:

$$l^{obs} = l_{on} \times [\text{NO}] \quad (7)$$

l_{off} was omitted simply because its value is very low, rendering the reaction virtually irreversible.

*Ma*Pgb(II)–NO was also obtained anaerobically by keeping the *Ma*Pgb(II) (1.3×10^{-6} M) solution under purified gaseous NO (760 mmHg), at pH 7.2 and 9.2 (1.0×10^{-1} M bis–tris propane buffer) and 22.0 °C.

All data were obtained between pH 7.2–9.5 (1.0×10^{-1} M bis–tris propane buffer) and 22.0 °C. The results are given as mean values of at least three experiments plus or minus the corresponding standard deviation. All data were analyzed using the matlab program (The Math Works Inc., Natick, MA, USA).

4. Results and discussion

Mixing of the *Ma*Pgb(III) and NO solutions at pH 7.2 induces a shift of the optical absorption maximum of the Soret band from 401 nm (i.e., *Ma*Pgb(III)) to 425 nm (i.e., *Ma*Pgb(III)–NO). Then, the *Ma*Pgb(III)–NO solution undergoes a slow shift of the optical absorption maximum of the Soret band from 425 nm (i.e., *Ma*Pgb(III)–NO) to 418 nm (i.e., *Ma*Pgb(II)–NO). The absorption spectra of *Ma*Pgb(III), *Ma*Pgb(III)–NO, and *Ma*Pgb(II)–NO are superimposable to those reported in the literature [3]. The reaction is irreversible as the spectrum of *Ma*Pgb(II)-NO reverts to *Ma*Pgb(II) instead of *Ma*Pgb(III) by pumping off gaseous NO from the *Ma*Pgb(II)–NO solution.

Under all the experimental conditions, the time course for *Ma*Pgb(III) reductive nitrosylation corresponds to a biphasic process (Fig. 1, panel A); values of k^{obs} and h^{obs} are wavelength-independent at fixed NO concentration. The first step of *Ma*Pgb(III) reductive nitrosylation (indicated by reaction *a* in Scheme 1) is a bimolecular process as observed under pseudo-first order conditions (Fig. 1, panel B). Plots of k^{obs} versus [NO] are linear (Eq. (4)), the slope and the *y* intercept corresponding to k_{on} and k_{off} values, respectively (see Table 1). From the dependence of the molar

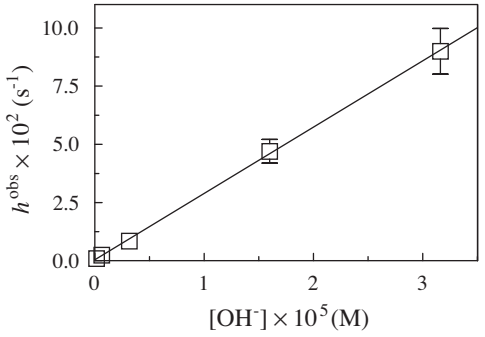

Fig. 2. Dependence of h^{obs} on [OH^-] for *Ma*Pgb(III) reductive nitrosylation. The continuous line was generated from Eqn. (6) with $h_{OH^-} = (2.9 \pm 0.3) \times 10^3$ M^{-1} s^{-1} and $h_{H_2O} = (4.1 \pm 0.4) \times 10^{-4}$ s^{-1}. Where not shown, standard deviation is smaller than the symbol. For details, see text.

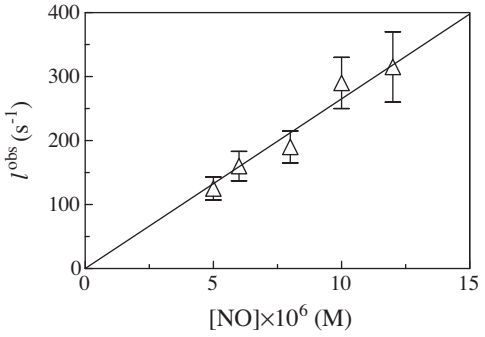

Fig. 3. Dependence of l^{obs} on [NO] for *Ma*Pgb(II) nitrosylation, at pH 7.2 and 22.0 °C. The continuous line was generated from Eq. (7) with l_{on}: = $(2.7 \pm 0.3) \times 10^7$ M^{-1} s^{-1}. The *Ma*Pgb(II) concentration was 1.3×10^{-6} M. Where not shown, standard deviation is smaller than the symbol. For details, see text.

Table 2
Values of kinetic and thermodynamic parameters for nitrosylation of ferric and ferrous heme–proteins[a].

Heme-protein		k_{on} (M^{-1} s^{-1})	k_{off} (s^{-1})	K (M)	k_{off}/k_{on} (M)	h_{OH^-} (M^{-1} s^{-1})	h_{H_2O} (s^{-1})	l_{on} (M^{-1} s^{-1})
*Ma*Pgb[b]		4.8×10^4	2.6	6.1×10^{-5}	5.4×10^{-5}	2.9×10^3	4.1×10^{-4}	2.7×10^7
G. max Lb[c]		1.4×10^5	3.0	2.1×10^{-5}	2.1×10^{-5}	3.3×10^3	3.0×10^{-4}	1.2×10^8
Sperm whale Mb[d]		1.9×10^5	1.4×10^1	7.7×10^{-5}	7.5×10^{-5}	3.2×10^2	n.d.	1.7×10^7
Human Ngb	fast phase	2.1×10^1[e]	2.5×10^{-3} [e]	n.d.	1.2×10^{-4} [f]	$\geqslant 2 \times 10^6$ [f]	n.d.	n.d. [g]
	slow phase	2.9 [e]	2.0×10^{-3} [e]	n.d.	1.9×10^{-4} [f]	$\geqslant 5 \times 10^5$ [f]	n.d.	n.d. [g]
Tetrameric human Hb[h]	α-chains	1.7×10^3	6.5×10^{-1}	8.3×10^{-5}	3.8×10^{-4}	3.2×10^3	1.1×10^{-3}	2.6×10^7
	β-chains	6.4×10^3	1.5	8.3×10^{-5}	2.3×10^{-4}	3.2×10^3	1.1×10^{-3}	2.6×10^7
Horse cytochrome *c*[i]		7.2×10^2	4.4×10^{-2}	6.1×10^{-5}	6.1×10^{-5}	1.5×10^3	n.d.	8.3
HSA–heme–Fe[j]		2.1×10^4	3.1×10^{-1}	1.8×10^{-5}	1.5×10^{-5}	4.4×10^3	3.5×10^{-4}	2.1×10^7
Rabbit HPX–heme–Fe[k]		1.3×10^1	$\leqslant 10^{-4}$	n.d.	$\leqslant 8 \times 10^{-6}$	$\geqslant 7 \times 10^5$	n.d.	6.3×10^3

n.d., not determined.
[a] All data were obtained between 10 °C and 22 °C. Values of K, k_{on}, k_{off}, k_{off}/k_{on}, and l_{on} were obtained between pH 6.5 and 7.5.
[b] Present study.
[c] From [20,35].
[d] From [17,18,36].
[e] From [19].
[f] Values of k_{off}, k_{off}/k_{on}, and h_{OH^-} were derived from [19].
[g] The l_{on} value for nitrosylation of the homologous ferrous mouse Ngb is 1.5×10^8 M^{-1} s^{-1} [37].
[h] From [18,38,39].
[i] From [17,18].
[j] From [22].
[k] From [21,40].

fraction of *Ma*Pgb(III) (i.e., α) on [NO] (Fig. 1, panel C), values of K were determined (see Table 1). As expected for simple systems [16], values of the Hill coefficient range between 0.98 ± 0.02 and 1.02 ± 0.02 (data not shown), and values of K agree with those of k_{off}/k_{on} (see Table 1). The second step (indicated by reaction *c* in Scheme 1) follows a [NO]-independent monomolecular behavior at all the pH values investigated (Fig. 1, panel D). According to Scheme 1, the value of h^{obs} is linearly-dependent on [OH^-] (Fig. 2, and Table 1). The slope and the *y* intercept of the plot of h^{obs} versus [OH^-] correspond to h_{OH^-} (= 2.9×10^3 M^{-1} s^{-1}) and h_{H_2O} (= 4.1×10^{-4} s^{-1}), respectively (see Table 1).

According to literature [3], addition of NO (either gaseous or dissolved in the buffer solution) to the *Ma*Pgb(II) solution brings about a shift in the maximum of the optical absorption spectrum in the Soret band from 432 nm (i.e., *Ma*Pgb(II)) to 418 nm (i.e., *Ma*Pgb(II)-NO).

Under all the experimental conditions, the time course for *Ma*Pgb(II) nitrosylation (see reaction *d* of Scheme 1) conforms grossly to a single-exponential decay. Values of l^{obs} are wavelength-independent at fixed NO concentration. Fig. 3 shows the linear dependence of l^{obs} for *Ma*Pgb(II) nitrosylation on [NO]. The analysis of data according to Eq. (7) allowed to determine values of l_{on} (see Table 1). The very fast NO binding to *Ma*Pgb(II) agrees with the fact that the *Ma*Pgb(II) species was never detected spectrophotometrically in the course of the *Ma*Pgb(III) reductive nitrosylation process.

The comparison of kinetic and thermodynamic parameters for *Ma*Pgb(III) reductive nitrosylation with those of other heme–proteins, reported in Table 2, allows the following considerations:

(i) Values of k_{on} and l_{on} for nitrosylation of ferric and/or ferrous *Ma*Pgb (present study), *Glycine max* leghemoglobin (*G. max* Lb) [20], sperm whale Mb [17,18], tetrameric human hemoglobin (Hb) [18], and HSA–heme–Fe [22] are higher than those reported for human neuroglobin (Ngb) [19], horse cytochrome *c* [17,18] and rabbit hemopexin–heme–Fe (HPX–heme–Fe) [21] (see Table 2). This reflects the relevance of heme coordination in the modulation of this process, since it turns out to be slower in six-coordinated heme–proteins, such as human Ngb, horse cytochrome *c*, and rabbit HPX–heme–Fe, which must undergo a transient six- to five-coordination to allow binding of exogenous ligands (e.g., NO) [24–26].

(ii) Values of k_{off} for NO dissociation from ferric nitrosylated heme–proteins span over five orders of magnitude (see Table 2), possibly reflecting the different stabilization geometry of the heme–Fe(III)–bound NO by heme distal amino acid residues [24–33].

(iii) Although values of k_{on} and k_{off} for NO binding to ferric heme–proteins span over several orders of magnitude (see Table 2), values of K (= k_{off}/k_{on}) are similar, indicating the occurrence of kinetic compensation phenomena.

(iv) Values of h_{OH^-} for reductive nitrosylation of human Ngb(III) and rabbit HPX–heme–Fe(III) [19,21] are larger by at least three orders of magnitude than those reported for *Ma*Pgb(III) (present study), *G. max* Lb(III) [20], sperm whale Mb(III) [17,18], human Hb(III) [18], horse cytochrome *c*(III) [17,18], and HSA–heme–Fe(III) [22] (see Table 2). This may reflect either different anion accessibility to the heme pocket or a difference of heme–protein reduction potentials [16,18,20,34]. Moreover, values of h_{OH^-} for ferric heme–protein nitrosylation are higher than those of h_{H_2O} by at least five orders of magnitude (see Table 2) indicating that OH^- ions catalyze the conversion of heme–Fe(II)–NO^+ to heme–Fe(II) (see reaction *c* in Scheme 1) much more efficiently than H_2O.

(v) Reductive nitrosylation of *Ma*Pgb (present study), *G. max* Lb(III) [20], sperm whale Mb(III) [17,18], human Hb(III) [18], and HSA–heme–Fe(III) [22] is limited by the OH^--mediated reduction of heme–Fe(II)–NO^+ to heme–Fe(II) (see reaction *c* in Scheme 1). On the other hand, NO binding to six-coordinated human Ngb(III), horse cytochrome *c*(III) and rabbit HPX–heme(III) (reaction *a* in Scheme 1) represents the rate-limiting step [18,19,21].

Present results highlight the role of *Ma*Pgb in the scavenging of reactive oxygen and nitrogen species which appears pivotal in the physiology of the strictly-anaerobic Archaea *M. acetivorans*. In fact, it is possible to envisage for *Ma*Pgb multiple functional roles, since its scavenging function(s) might coexist with an enzymatic

activity(ies) to facilitate the conversion of CO to methane, being an adaptation to different gaseous environments.

Acknowledgments

This work was partially supported by grants from Ministero dell'Istruzione, dell'Università e della Ricerca of Italy (MiUR PRIN 2007SFZXZ7_002 to M.C., MiUR PRIN 20109MXHMR_001 to P.A., and University Roma Tre, CLAR 2012 to P.A.).

References

[1] S. Hou, T. Freitas, R.W. Larsen, M. Piatibratov, V. Sivozhelezov, A. Yamamoto, E.A. Meleshkevitch, M. Zimmer, G.W. Ordal, M. Alam, Globin-coupled sensors: a class of heme-containing sensors in Archaea and Bacteria, Proc. Natl. Acad. Sci. USA 98 (2001) 9353–9358.
[2] T.A.K. Freitas, S. Hou, M. Alam, The diversity of globin-coupled sensors, FEBS Lett. 552 (2003) 99–104.
[3] T.A.K. Freitas, S. Hou, E.M. Dioum, J.A. Saito, J. Newhouse, G. Gonzalez, M.A. Gilles-Gonzalez, M. Alam, Ancestral hemoglobins in Archaea, Proc. Natl. Acad. Sci. USA 101 (2004) 6675–6680.
[4] T.A.K. Freitas, J.A. Saito, S. Hou, M. Alam, Globin-coupled sensors, protoglobins, and the last universal common ancestor, J. Inorg. Biochem. 99 (2005) 23–33.
[5] S.N. Vinogradov, D. Hoogewijs, X. Bailly, R. Arredondo-Peter, J. Gough, S. Dewilde, L. Moens, J.R. Vanfleteren, A phylogenomic profile of globins, BMC Evol. Biol. 6 (2006) 31.
[6] S.N. Vinogradov, D. Hoogewijs, X. Bailly, K. Mizuguchi, S. Dewilde, L. Moens, A model of globin evolution, Gene 398 (2007) 132–142.
[7] M. Nardini, A. Pesce, L. Thijs, J.A. Saito, S. Dewilde, M. Alam, P. Ascenzi, M. Coletta, C. Ciaccio, L. Moens, M. Bolognesi, Archaeal protoglobin structure indicates new ligand diffusion paths and modulation of haem-reactivity, EMBO Rep. 9 (2008) 157–163.
[8] A. Pesce, L. Tilleman, S. Dewilde, P. Ascenzi, M. Coletta, C. Ciaccio, S. Bruno, L. Moens, M. Bolognesi, M. Nardini, Structural heterogeneity and ligand gating in ferric *Methanosarcina acetivorans* protoglobin mutants, IUBMB Life 63 (2011) 287–294.
[9] F. Forti, L. Boechi, D. Bikiel, M.A. Martí, M. Nardini, M. Bolognesi, C. Viappiani, D. Estrin, F.J. Luque, Ligand migration in *Methanosarcina acetivorans* protoglobin: effects of ligand binding and dimeric assembly, J. Phys. Chem. B. 115 (2011) 13771–13780.
[10] E. Oelgeschläger, M. Rother, Carbon monoxide-dependent energy metabolism in anaerobic bacteria and archaea, Arch. Microbiol. 190 (2008) 257–269.
[11] S. Abbruzzetti, L. Tilleman, S. Bruno, C. Viappiani, F. Desmet, S. Van Doorslaer, M. Coletta, C. Ciaccio, P. Ascenzi, M. Nardini, M. Bolognesi, L. Moens, S. Dewilde, (2012) Ligation tunes protein reactivity in an ancient haemoglobin: kinetic evidence for an allosteric mechanism in *Methanosarcina acetivorans* protoglobin, PLoS One 7 (2012) e33614.
[12] M. Rother, W.W. Metcalf, Anaerobic growth of *Methanosarcina acetivorans* C2A on carbon monoxide: an unusual way of life for a methanogenic archaeon, Proc. Natl. Acad. Sci. USA 101 (2004) 16929–16934.
[13] D.J. Lessner, L. Li, T. Eejtar, V.P. Andreev, M. Reichlen, K. Hill, J.J. Moran, B.L. Karger, J.G. Ferry, An unconventional pathway for reduction of CO_2 to methane in CO-grown *Methanosarcina acetivorans* revealed by proteomics, Proc. Natl. Acad. Sci. USA 103 (2006) 17921–17926.
[14] J.G. Ferry, C.H. House, The stepwise evolution of early life driven by energy conservation, Mol. Biol. Evol. 23 (2006) 1286–1296.
[15] S. Dewilde, L. Kiger, T. Burmester, T. Hankeln, V. Baudin-Creuza, T. Aerts, M.C. Marden, R. Caubergs, L. Moens, Biochemical characterization and ligand binding properties of neuroglobin, a novel member of the globin family, J. Biol. Chem. 276 (2001) 38949–38955.
[16] E. Antonini, M. Brunori, Hemoglobin and Myoglobin in their Reactions with Ligands, North-Holland Publishing Co, Amsterdam, 1971.
[17] M. Hoshino, K. Ozawa, H. Seki, P.C. Ford, Photochemistry of nitric oxide adducts of water-soluble iron(III) porphyrin and ferrihemoproteins studied by nanosecond laser photolysis, J. Am. Chem. Soc. 115 (1993) 9568–9575.
[18] M. Hoshino, M. Maeda, R. Konishi, H. Seki, P.C. Ford, Studies on the reaction mechanism for reductive nitrosylation of ferrihemoproteins in buffer solutions, J. Am. Chem. Soc. 118 (1996) 5702–5707.
[19] S. Herold, A. Fago, R.E. Weber, S. Dewilde, L. Moens, Reactivity studies of the Fe(III) and Fe(II)NO forms of human neuroglobin reveal a potential role against oxidative stress, J. Biol. Chem. 279 (2004) 22841–22847.
[20] S. Herold, A. Puppo, Kinetics and mechanistic studies of the reactions of metleghemoglobin, ferrylleghemoglobin, and nitrosylleghemoglobin with reactive nitrogen species, J. Biol. Inorg. Chem. 10 (2005) 946–957.
[21] P. Ascenzi, A. Bocedi, G. Antonini, M. Bolognesi, M. Fasano, Reductive nitrosylation and peroxynitrite-mediated oxidation of heme–hemopexin, FEBS J. 274 (2007) 551–562.
[22] P. Ascenzi, Y. Cao, A. di Masi, F. Gullotta, G. De Sanctis, G. Fanali, M. Fasano, M. Coletta, Reductive nitrosylation of ferric human serum heme–albumin, FEBS J. 277 (2010) 2474–2485.
[23] H. Bateman, Solution of a system of differential equations occurring in the theory of radioactive transformations, Proc. Cambridge Philos. Soc. 15 (1910) 423–427.
[24] L. Banci, I. Bertini, J.G. Huber, G.A. Spyroulias, P. Turano, Solution structure of reduced horse heart cytochrome *c*, J. Biol. Inorg. Chem. 4 (1999) 21–31.
[25] M. Paoli, B.F. Anderson, H.M. Baker, W.T. Morgan, A. Smith, E.N. Baker, Crystal structure of hemopexin reveals a novel high-affinity heme site formed between two ß-propeller domains, Nat. Struct. Biol. 6 (1999) 926–931.
[26] A. Pesce, S. Dewilde, M. Nardini, L. Moens, P. Ascenzi, T. Hankeln, T. Burmester, M. Bolognesi, Human brain neuroglobin structure reveals a distinct mode of controlling oxygen affinity, Structure 11 (2003) 1087–1095.
[27] M.F. Perutz, Myoglobin and haemoglobin: role of distal residues in reactions with haem ligands, Trends Biochem. Sci. 14 (1989) 42–44.
[28] E.H. Harutyunyan, T.N. Safonova, I.P. Kuranova, A.N. Popov, A.V. Teplyakov, G.V. Obmolova, B.K. Valnshtein, G.G. Dodson, J.C. Wilson, The binding of carbon monoxide and nitric oxide to leghaemoglobin in comparison with other haemoglobins, J. Mol. Biol. 264 (1996) 152–161.
[29] A.E. Miele, S. Santanché, C. Travaglini-Allocatelli, B. Vallone, M. Brunori, A. Bellelli, Modulation of ligand binding in engineered human hemoglobin distal pocket, J. Mol. Biol. 290 (1999) 515–524.
[30] E.A. Brucker, J.S. Olson, M. Ikeda-Saito, G.N. Phillips Jr, Nitric oxide myoglobin: crystal structure and analysis of ligand geometry, Proteins 30 (1998) 352–356.
[31] N.L. Chan, J.S. Kavanaugh, P.H. Rogers, A. Arnone, Crystallographic analysis of the interaction of nitric oxide with quaternary-T human hemoglobin, Biochemistry 43 (2004) 118–132.
[32] F.P. Nicoletti, B.D. Howes, M. Fittipaldi, G. Fanali, M. Fasano, P. Ascenzi, G. Smulevich, Ibuprofen induces an allosteric conformational transition in the heme complex of human serum albumin with significant effects on heme ligation, J. Am. Chem. Soc. 130 (2008) 11677–11688.
[33] G. Fanali, A. di Masi, V. Trezza, M. Marino, M. Fasano, P. Ascenzi, Human serum albumin: from bench to bedside, Mol. Aspects Med. 33 (2012) 209–290.
[34] J.G. Beetlestone, O.S. Adeosun, J.E. Goddard, J.B. Kushimo, M.M. Ogunlesi, G.B. Ogunmola, K.O. Okonjo, B. Seamonds, Reactivity difference between haemoglobins Part XIX, J. Chem. Soc. Dalton Trans. (1976) 1251–1278.
[35] R.J. Rohlfs, J.S. Olson, Q.H. Gibson, A comparison of the geminate recombination kinetics of several monomeric heme proteins, J. Biol. Chem. 263 (1988) 1803–1813.
[36] E.G. Moore, Q.H. Gibson, Cooperativity in the dissociation of nitric oxide from hemoglobin, J. Biol. Chem. 251 (1976) 2788–2794.
[37] S. Van Doorslaer, S. Dewilde, L. Kiger, S.V. Nistor, E. Goovaerts, M.C. Marden, L. Moens, Nitric oxide binding properties of neuroglobin. A characterization by EPR and flash photolysis, J. Biol. Chem. 278 (2003) 4919–4925.
[38] R. Cassoly, Q. Gibson, Conformation, co-operativity and ligand binding in human hemoglobin, J. Mol. Biol. 91 (1975) 301–313.
[39] V.S. Sharma, T.G. Traylor, R. Gardiner, H. Mizukami, Reaction of nitric oxide with heme proteins and model compounds of hemoglobin, Biochemistry 26 (1987) 3837–3843.
[40] M. Fasano, A. Bocedi, M. Mattu, M. Coletta, P. Ascenzi, Nitrosylation of rabbit ferrous heme–hemopexin, J. Biol. Inorg. Chem. 9 (2004) 800–806.